Ultrasonic Glued Wood Finger-jointed Panel Quality Inspection System with Barker Code Pulse Excitation

Jie Chen,[a] Yongning Yuan,[a] Daipeng Fu,[c] Jun Wang,[b] Hongyan Zou,[a] Liang Qi,[a] and Zheng Wang [c,*]

Glued wood finger-jointed panels are widely employed due to their efficient use of wood resources and the enhancement of product quality. To address defects in the quality inspection of these panels, a set of ultrasonic glued laminated wood finger-joined board inspection systems was designed using Barker Code pulse excitation. This was achieved by adopting air-coupled ultrasonic technology and incorporating phase coding technology. Relevant validation experimental research was carried out on the performance of the system. The results show that the system covered two key components, namely hardware and software, which enabled its ultrasonic transducer to realise the functions of rapid scanning of the internal and external qualities of the board and automatic C-scan inspection imaging to identify defects in the specimen without contacting the glued wood finger-joined board specimen. The validation test confirmed that the inspection system achieved good accuracy and reliability. It was concluded that this approach has potential to improve the quality inspection technology of glued laminated direct lumber and to promote the development of wood processing industry.

DOI: 10.15376/biores.20.2.2887-2903

Keywords: Glued wood finger-joined boards; Ultrasonic; Barker code pulse excitation; Quality inspection system; Spline interpolation algorithm

*Contact information: a: College of Mechanical and Electronic Engineering, Nanjing Forestry University, Nanjing, 210037, China; b: College of Information Science and Technology, Nanjing Forestry University, Nanjing, 210037, China; c: College of Materials Science and Engineering, Nanjing Forestry University, Nanjing, 210037, China; *Corresponding author: wangzheng63258@163.com*

INTRODUCTION

In the field of wood processing, defects, such as knots, cracking, mold, rot, insect damage, grain irregularities, and blunt edges, can significantly impact the quality of sawn timber. These issues affect both the processing and usage of sawn timber. An effective solution to these problems is the use of finger-jointing and splicing technology to produce glued wood finger-jointed panels. These panels are made by joining multiple boards together, which optimizes wood resource usage, enhances quality, and reduces waste. Finger-jointed lumber pieces and panels are widely used in various industries, including wood-frame construction, furniture, interior decoration, transportation, military applications, and musical instruments (Zhou *et al*. 2021).

With the rapid advancement of industrial technology, various inspection methods have emerged in wood processing, including ultrasonic, stress wave, and vibration techniques. Probabilistic methods have been used to study mechanical properties of materials (Wang and Ghanem 2021, 2022, 2023; Yu *et al*. 2023). In non-contact ultrasonic detection, phase coding methods, such as Barker code, Taylor code, and M sequences, are

commonly used (Ghavamirad *et al.* 2018; Murata and Kaneda 2019). The Barker code, known for its excellent noise suppression and autocorrelation properties, offers significant advantages such as strong anti-jamming capability, high resolution, bandwidth efficiency, ease of identification, and high system performance. This makes it highly promising for ultrasonic detection in wood.

For example, in 2015, Sanabria et al. established a reliable nondestructive ultrasonic system for inspecting wood composite structures by constructing a time-domain finite-difference (FDTD) model. This model incorporated local anisotropic variations in stiffness, damping, and density to effectively detect wood properties (Sanabria *et al.* 2015). In 2019, Ahmad utilized Barker Code Thermal Wave Imaging for nondestructive testing (NDT) of steel materials and compared it with conventional thermal NDT methods, demonstrating that the technique offers higher contrast and signal-to-noise ratios (Ahmad *et al.* 2019). In 2021, Maldaner developed a system integrating photoelectric sensors, ultrasonic sensors, and encoders to detect and map plants in sugarcane rows using machine learning modeling. This system proved effective in accurately detecting plants within sugarcane rows (Maldaner *et al.* 2021). In 2023, Parvez employed Barker encoded thermal wave imaging to identify anomalies in various materials. This method achieved a high signal-to-noise ratio (SNR) of 108 dB and improved the reliability of thermal imaging detection by identifying smaller defects at greater depths, even in fully corroded mild steel samples (Parvez *et al.* 2023).

Given the increasing demand for wood, it is crucial to advance research and development in high-level nondestructive testing and evaluation systems to enhance wood utilization. This paper applies the Barker code phase coding pulse compression technique to non-contact ultrasonic inspection of wood to improve the signal-to-noise ratio of measurement signals. This method is particularly suited for detecting internal defects in wood and offers advantages, such as rapid detection, accuracy, reliability, and no pollution hazards, making it suitable for use in forest areas.

EXPERIMENTAL

Principles of Transmissive C-Scan and Phase-Encoded Pulse Compression Techniques

Transmission C-scan

Ultrasonic C-scanning is an advanced automated inspection technology that integrates ultrasonic detection, motion control, and image display processing. The principle of this technology is illustrated in Fig. 1. During the ultrasonic C-scan process, an ultrasonic signal is emitted from a transmitter-end transducer at the start of a predetermined detection area on the sample. The signal travels through the air medium to the designated sampling point, passes through the sample, and then returns to the air, where it is finally received by the receiver-end transducer.

The received signal is then processed to extract amplitude and time data, which are used as imaging parameters. The scanning line is followed to detect all remaining sampling points in the area. Once the scanning is complete, the collected data are visualized to reveal the morphological characteristics and dimensions of any defects, allowing for the differentiation of various types of defects.

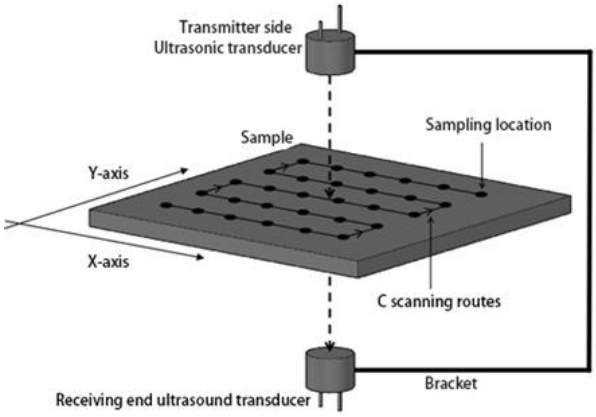

Fig. 1. Ultrasound C-scan

Phase-encoded pulse compression technique

The basic principle of pulse compression technology involves converting long pulses into short pulses using specific signal processing algorithms, thereby achieving higher range resolution. In conventional radar systems, long pulses are used for detecting long-range targets, but this often results in lower range resolution. Pulse compression techniques address this by utilizing the phase and amplitude information of the pulses and performing complex processing at the receiving end. This conversion enhances range resolution in the time domain, allowing radar systems to more accurately determine the distance between targets. This technique significantly enhances radar system performance, enabling better adaptation to a wide range of environmental conditions and target characteristics. Studies have demonstrated that applying pulse compression in air-coupled ultrasonic detection can significantly improve the signal-to-noise ratio of the received signal, making the main peak of the signal more distinguishable (Arkhipov *et al.* 2021; Bruder *et al.* 2021).

(1) Principle of phase coding pulse compression technology

Currently, frequency modulation pulse compression techniques are widely used in the field of ultrasonic detection. These techniques involve complex signal pre-processing and can result in a relatively low signal-to-noise ratio, making signal analysis more challenging. However, phase coding techniques offer considerable advantages in this context. The signal of 7-bit sinusoidal Barker code is shown in Fig. 2.

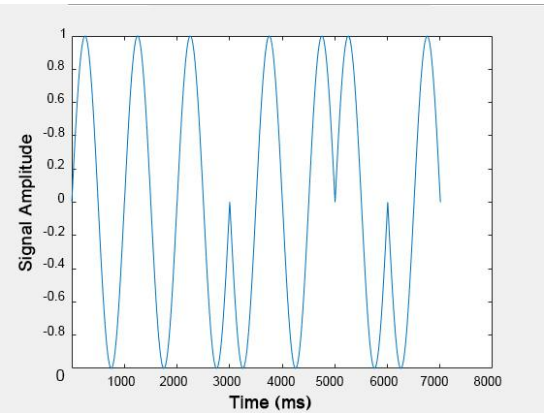

Fig. 2. 7-bit Barker code signal

Figure 3 illustrates the autocorrelation of the 7-bit Barker code, which demonstrates a high primary-to-secondary lobe ratio and significantly prominent peak characteristics. This property effectively suppresses noise interference (Han *et al.* 2019; Soner *et al.* 2020). In this study, the phase-coded pulse compression technique is employed to image the received signal's peak voltage by collecting and processing the data (Zhang *et al.* 2020; Li *et al.* 2021), this method emphasizes the main peak characteristics of the signal, thereby significantly enhancing imaging accuracy.

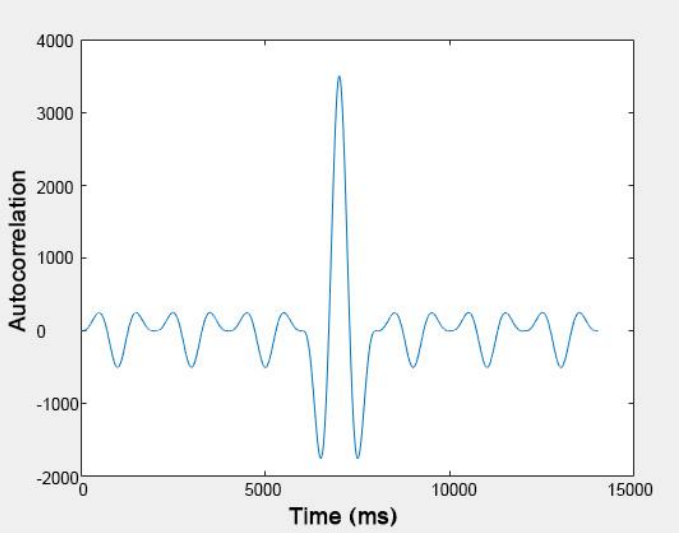

Fig. 3. Autocorrelation of 7-bit Barker code

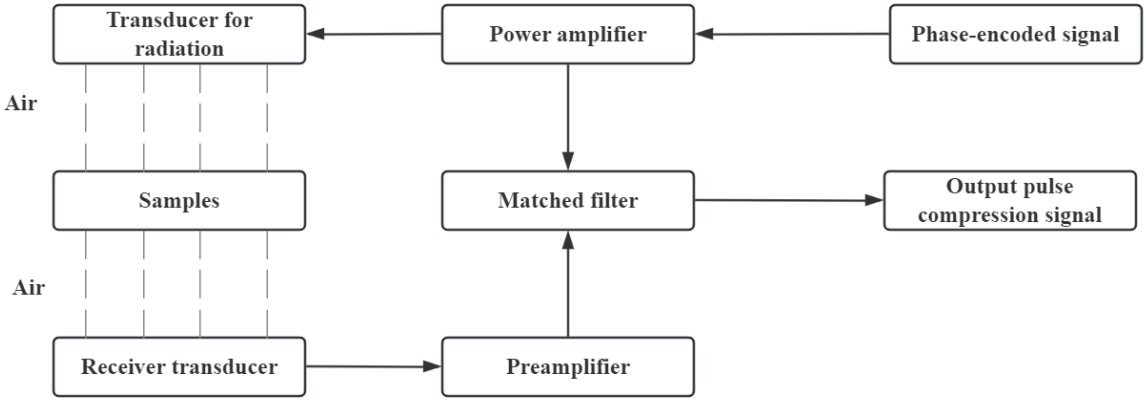

Fig. 4. Schematic diagram of phase coding technology

(2) Comsol simulation analysis of Barker code pulse ultrasonic wood detection

The transmission and reception models of the 7-bit sine wave signal and 7-bit Barker code signal were established in COMSOL, as depicted in Fig. 5. In this setup, ultrasonic transducers are placed symmetrically, with the transmitting transducer at the lower end and the receiving transducer at the upper end. The system operates at a frequency of 40 kHz. The transmitting transducer emits ultrasonic waves, which propagate through the air, experience attenuation, and eventually reach the receiving transducer. The receiving transducer then captures the ultrasonic signals.

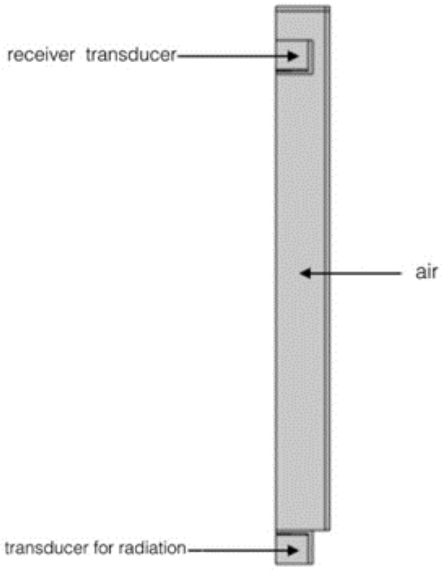

Fig. 5. Ultrasonic emission and reception model

Figure 6 displays the received signal diagrams for both the sine wave and Barker code signals. The sine wave signal, due to its simpler structure, is more prone to noise interference, which can lead to information loss or errors. In contrast, the Barker code pulse signal exhibits superior anti-interference capabilities due to its unique coding method. This method effectively suppresses noise interference, thereby enhancing the reliability and stability of the signal. Additionally, the Barker code pulse signal features a distinct main peak characteristic at the receiving end, which improves the signal-to-noise ratio and resolution. This allows for precise detection and analysis of the signal.

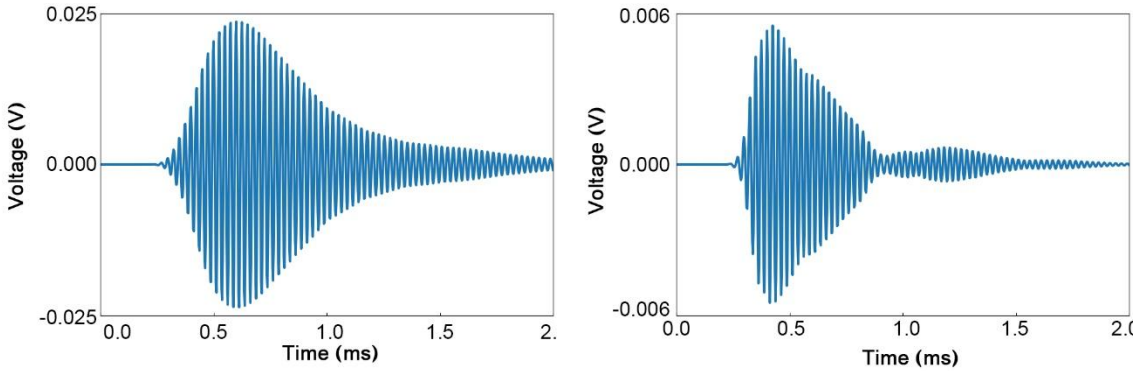

(a) Sine wave receive signal **(b)** Barker code receiving signal

Fig. 6. Acceptance diagram for both signals

System Software and Hardware Design

System hardware design

The overall block diagram of the hardware of the ultrasonic detection of plywood fingerboard quality inspection system with Barker code pulse excitation is shown in Fig. 7.

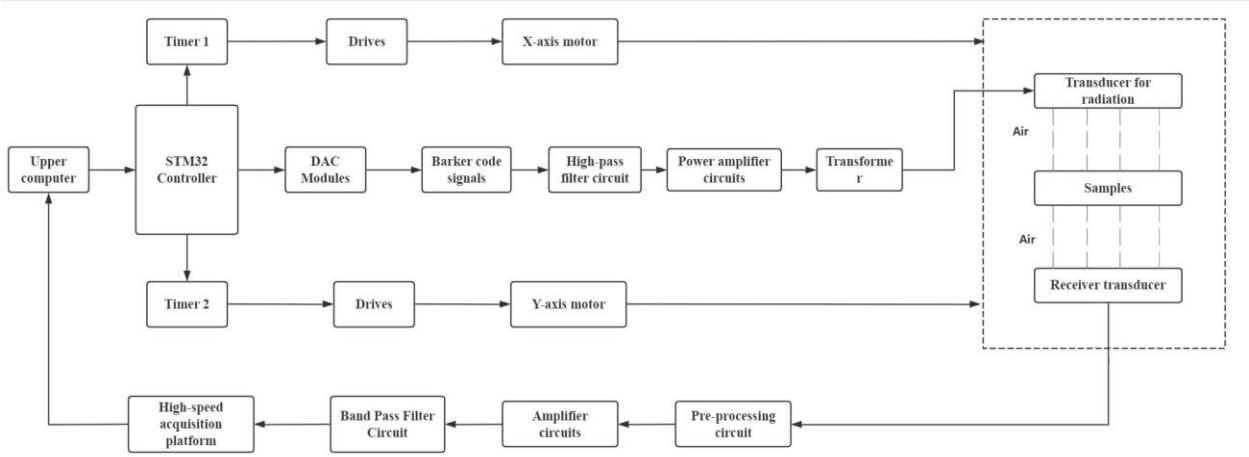

Fig. 7. Detection system hardware design diagram

The motion control module of this system primarily consists of a dual axis scanning platform, an operation interface, a main controller, and stepping motors. Users set the motion parameters *via* the host computer's operation interface and send commands to the main controller. The main controller then regulates the motion of the dual-axis stepping motors to perform the C-scan. The dual-axis scanning platform is designed with three drive motors positioned along the X-axis and Y-axis to carry the ultrasonic transducer for ultrasonic C-scanning detection. Two stepping motors along the X-axis are synchronized to the same control signal, while a single control signal governs the Y-axis motor. This configuration allows for precise control of the three stepping motors, enabling the ultrasonic detection process. The scanning control flow is illustrated in Fig. 8.

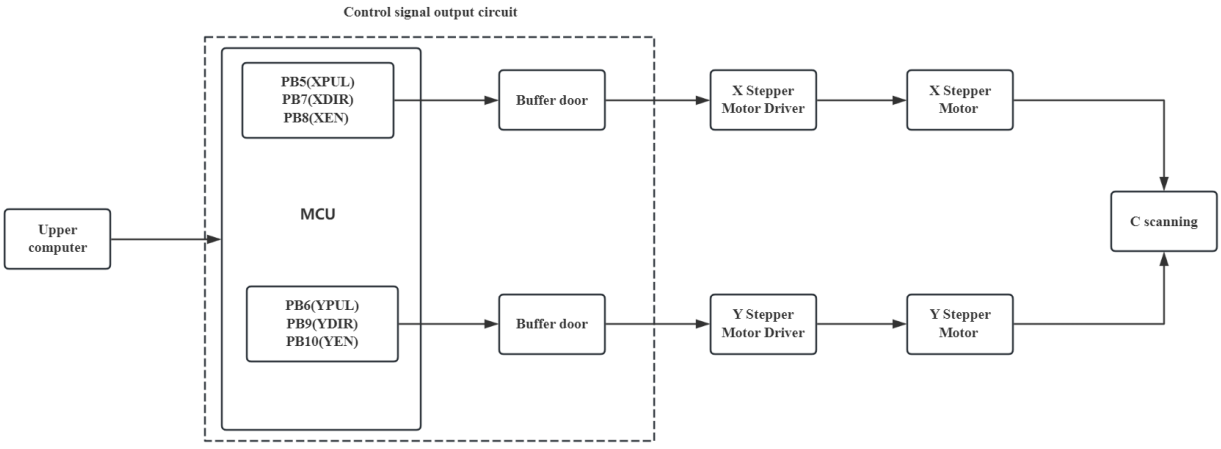

Fig. 8. C-scan control flow

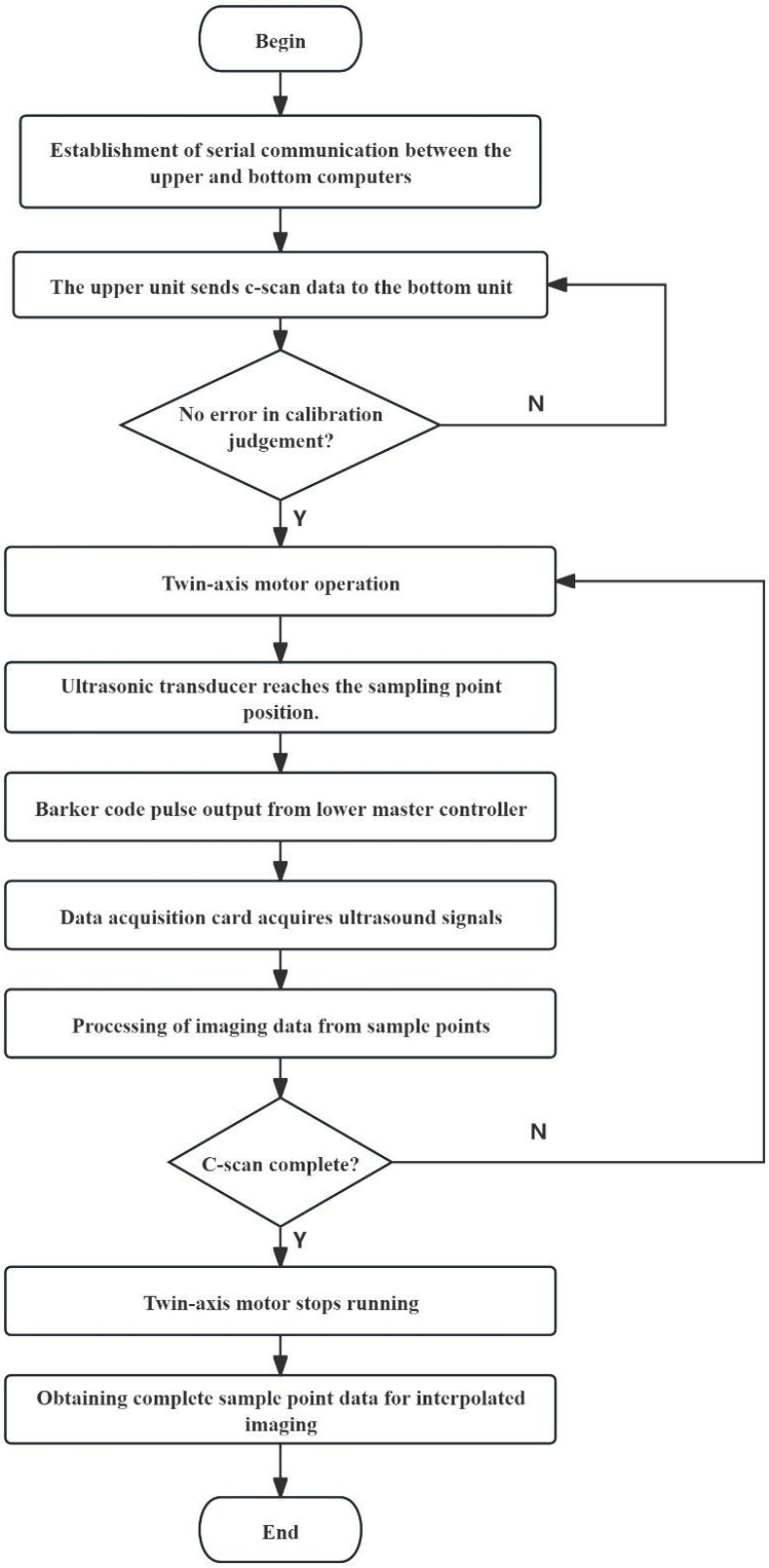

Fig. 9. System software design flow chart

System software design

The software design of this quality inspection system includes: user interface, serial communication, motion control system, Barker Code pulse output, signal acquisition, signal processing, and imaging system. The system software design flow chart is shown in Fig. 9.

This system belongs to the field of embedded system development, which uses serial port connection to achieve programme downloading, debugging, and testing with the target embedded system, as well as interacting with external devices. This serial communication method provides a simple and reliable data transmission mechanism. In this system, serial communication also undertakes the important tasks of remote control, monitoring, and debugging of devices and systems. Specifically, it is responsible for controlling the motor movement to complete the C-scan function and receiving the data captured by the data acquisition card in real time for imaging processing. This implementation of serial communication is fast and efficient, effectively improving the performance of the system.

Data imaging design

In image processing algorithms, directly converting raw data into images often results in a lack of smooth transitions between image pixels. This issue is particularly problematic in wood inspection, as it can hinder the accurate localization of defects. To address this, the system employs interpolation methods to refine the transitions between pixel points (Xu *et al.* 2020; Wang *et al.* 2020). The most commonly used algorithm is the multi-order multinomial spline difference algorithm, which constructs smooth curves or surfaces over a given set of data points. This algorithm provides excellent smoothness, avoids abrupt fluctuations caused by large gaps between data points, and offers high accuracy and wide applicability. It can process one-dimensional, two-dimensional, or even higher-dimensional data, yielding highly accurate interpolation results and accurately reconstructing the shape of curves or surfaces.

However, the multi-order multinomial spline difference algorithm has limitations, including high computational complexity and significant data requirements. This complexity demands more computational resources and time, especially when handling large datasets. To ensure computational efficiency, this paper primarily utilizes a low-order spline interpolation algorithm. This approach maintains an effective balance between computational complexity and interpolation error while preserving the desired interpolation effects.

Spline interpolation essentially involves interpolating between multiple line segments in a discontinuous manner to achieve smooth curve transitions, thereby approximating the actual data trends more coherently. The core concept of spline interpolation is to approximate discrete data points effectively by introducing a sufficient number of interpolation nodes. This ensures that the curve achieves a high degree of smoothness within the interpolation interval and maintains a certain level of continuity in the derivative at the interpolation nodes. The division is performed within the set [a, b] region.

$$\Delta : a = x_0 < x_1 < \cdots < x_{n-1} < x_n = b \tag{1}$$

The step function is a zeroth spline function:

$$S_0(x) = a_0 + \sum b_j (x - x_j)_+^0 \tag{2}$$

The kth order spline function is obtained by integrating S0 (x) k times:

$$S_k(x) = \sum_{j=0}^{k} \frac{a_j x^j}{j!} + \sum_{j=1}^{n-1} \frac{b_j (x - x_j)_+^k}{k!} \quad (3)$$

Cubic spline function:

$$S_3(x) = a_0 + a_1 x + \frac{a_2 x^2}{2!} + \frac{a_3 x^3}{3!} + \sum_{j=1}^{n-1} \frac{b_j (x - x_j)_+^3}{3!} \quad (4)$$

The cubic spline function is widely used in various fields for accurate data fitting and smooth approximation due to its high efficiency and reliability (Hu *et al.* 2021; Cao *et al.* 2023). In this study, to determine the optimal interpolation scheme, first-order linear interpolation, third-order spline interpolation, and fifth-order spline interpolation were applied to the original data. These interpolation methods provide finer approximations of the original data, resulting in more accurate and smoother representations of the 2D data. Through observing and comparing these three interpolation methods, it is possible to gain insights into the performance of different interpolation algorithms in image processing, offering a more reliable basis for data analysis. Figure 10 illustrates the imaging effects of the three interpolation methods.

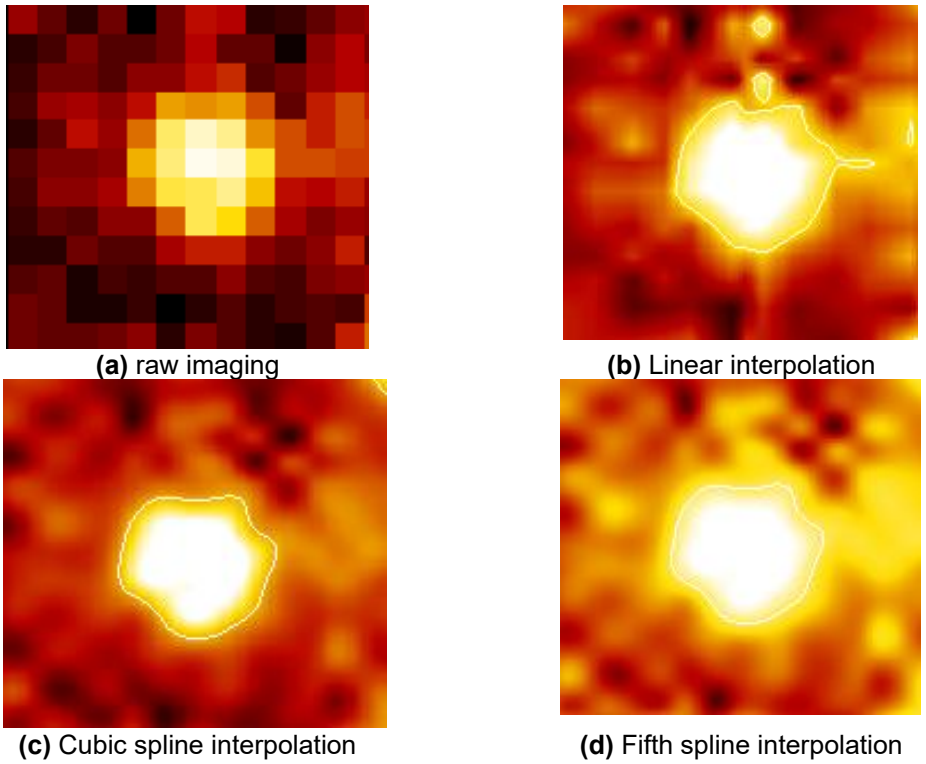

(a) raw imaging **(b)** Linear interpolation

(c) Cubic spline interpolation **(d)** Fifth spline interpolation

Fig. 10. Three types of interpolation imaging maps

In this study, three different interpolation methods were evaluated for image interpolation. Linear interpolation demonstrated the worst performance in terms of smoothness, particularly struggling with datasets containing rapid changes or non-linear relationships. Five-times spline interpolation, while providing more detail, proved unstable and susceptible to sudden changes near the boundaries, resulting in poor imaging quality.

Additionally, the computational demands of five-times spline interpolation were high, significantly increasing the imaging time.

In contrast, three-times (cubic) spline interpolation provided excellent image smoothness and avoided the emergence of distorted regions. It also performed well in terms of computational efficiency, significantly reducing the imaging time. After comprehensive consideration, the system opted for cubic spline interpolation to process the original imaging data, balancing smoothness and computational efficiency. Interpolation is less effective if there are rapid changes or non-linear relationships in the dataset.

Performance Verification of the Detection System

The ultrasonic glued wood finger-jointed board quality inspection system with Barker code pulse excitation designed in this paper is shown in Fig. 11.

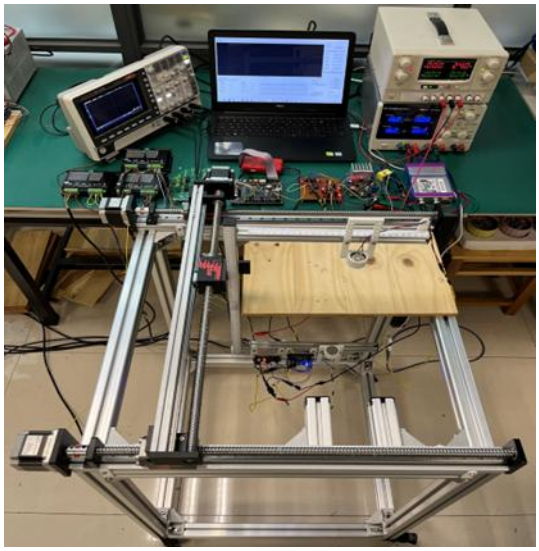

Fig. 11. Detection system

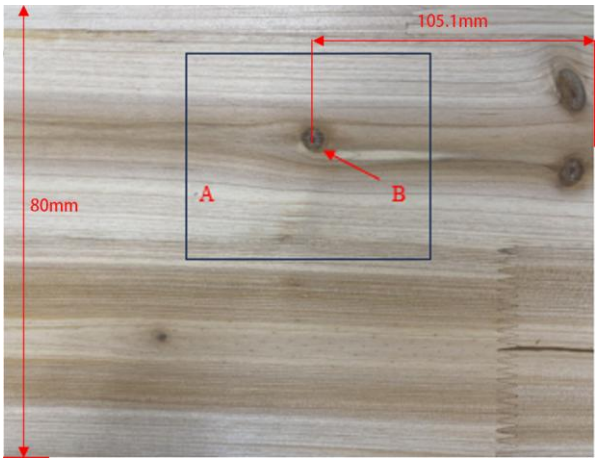

Fig. 12. node defects

Nodule Testing

Determining the test sample and testing parameters

In this study, three defect-free specimens were selected and designated as W-1, W-2, and W-3; in addition, three specimens exhibiting knots and internal cavities were labeled Y-1, Y-2, and Y-3. The specifications for both types of specimens are detailed in Table 1. Figure 12 illustrates specimen Y-1 of the glued laminated timber finger joint. This specimen measured 400mm×80mm×8.47mm, with the detection area defined by the black-framed section in the figure measuring 50mm×50mm×9mm. Prior to conducting C-scan imaging, it is essential to accurately position the probe at locations A and B to perform A-scan measurements. The amplitudes of signals obtained from these two points are subsequently analyzed to ensure precision in data acquisition by the system. Through a series of iterative trials, it was determined that a gain setting of 63dB was optimal for subsequent C-scan imaging.

Mechanical Property Verification Test

For the detection results of internal defects in the system, it is necessary to evaluate the accuracy. Usually, the defect of the sample is sawed to see if it is consistent with the test results, and this method can cause damage to the wood. In this study, dynamic mechanical properties experiment was chosen to verify the accuracy of the designed system without causing damage to the wood itself (Corbi *et al.* 2021; Olonisakin *et al*. 2022; Adegbemileke *et al*. 2024; Shavir *et al*. 2024).

Testing principle and procedure

The free plate transient excitation method is based on the transverse bending theory of Euler beam (Wang *et al.* 2018, 2019). Through applying an external shock to the test object to stimulate its vibration, the vibration frequency is collected and the first-order bending frequency is obtained using Eq. 5 to obtain the value of the modulus of elasticity of the specimen,

$$E = 0.9462\rho\frac{l^4 f_{1b}^2}{h^2} \quad (5)$$

where E is the dynamic modulus of elasticity value (Pa); ρ is the dry gas density (kg/m^3); f_{1b} is the first-order bending frequency value of the free beam (Hz); l is the length of the beam (m); and h is the thickness of the beam (m).

The main testing steps were as follows: First, a free beam configuration was achieved by hanging the elastic cord at a distance of 0.224L and 0.776L from the end of the glued laminated timber jointed plate specimen. A sound level meter was placed 10 mm below the corner points of the plate specimen, and the CRAS vibration and dynamic signal acquisition and analysis system was connected to the SsCras signal analysis software (Wang *et al.* 2014, 2016). The instrument consisted of a signal conditioning box, a signal acquisition box, the SsCras analysis software, and a computer. Second, the plate specimen was excited by tapping the corner points to produce free vibrations, and the acceleration sensor receives the vibration signal and converts it into an electrical signal output. The electrical signal was amplified, filtered, and converted to a digital signal through an A/D converter to obtain the spectrum and the first-order bending frequency of the specimen (Wang *et al.* 2015). Finally, the elastic modulus E of the specimen was calculated using Eq. 5.

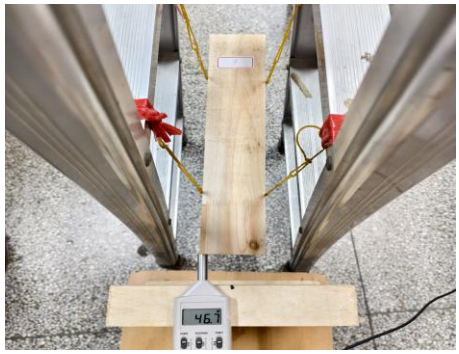

Fig. 13. Experimental site

Test Results and Analysis

Nodule analysis of test results

Figure 14 shows the detection signals at point A and point B. Relative to point A, the obvious signal attenuation and even received signal reduction results at point B, the root cause is that it contained a high density of nodes.

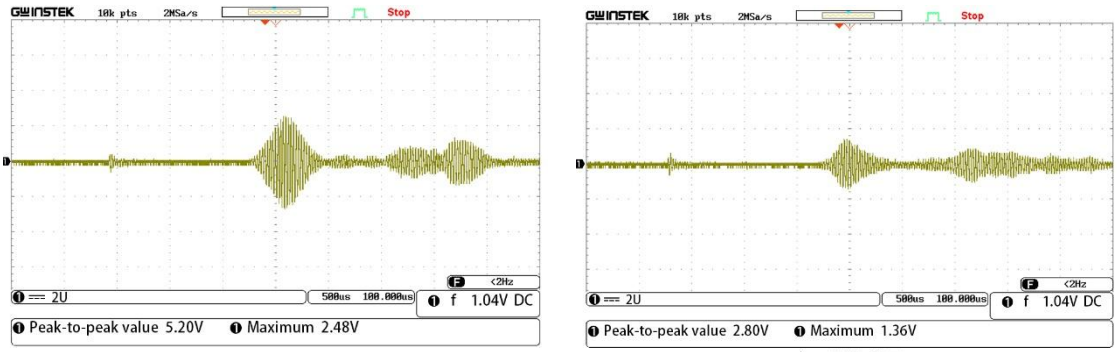

(a) Signal detected at A **(b)** Signal detected at B

Fig. 14. Signal detection

In Fig. 14, the C-scan imaging results clearly show that the regions with nodules were represented by dark black areas, indicating relatively low amplitudes, while other areas display yellowish-white results corresponding to higher amplitudes. This observation aligns with the theoretical analysis.

The inspection system designed in this study performs effectively in detecting knot defects in plywood finger-jointed boards. It accurately locates and outlines the shapes of knot defects, demonstrating the system's excellent performance in this area.

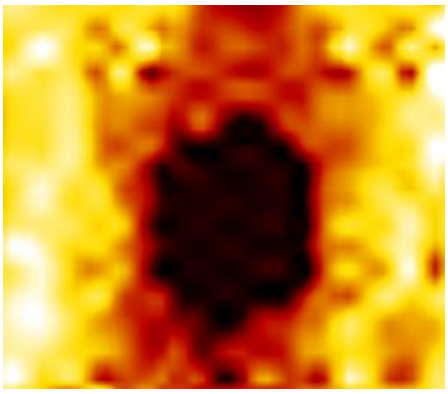

Fig. 15. Imaging of nodal defects

Internal cavity detection

In this study, internal defects in glued laminated wood finger-jointed panels were detected and imaged by C-scan. After C-scan detection of 30 pieces of glued laminated wood finger-joined panels with dimensions of 450 m×250 mm×9 mm, several specimens that contained internal defects were detected. The detection signal of one of the test pieces is shown in Fig. 15.

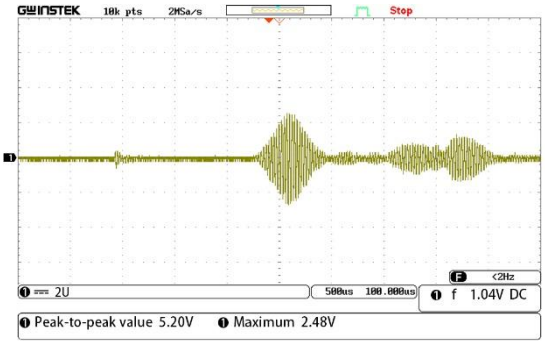

(a) Detection signal at no defects

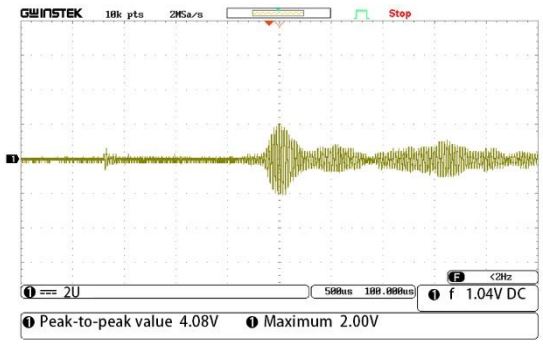

(b) Detection signal at defects with internal cavities

Fig. 16. Signal detection

When the ultrasonic signal encounters an internal cavity, it undergoes a dielectric transition, leading to energy attenuation. As a result, the amplitude of the detected signal is lower in regions with internal defects compared to defect-free areas. In contrast to the defect-free regions, the imaging of internal cavity defects exhibited a strikingly bright white tone, making the defects more prominent in the imaging data. However, due to the relatively thin nature of the internal cavity defects, the ultrasonic signal experienced only slight attenuation as it passed through the board, resulting in a higher amplitude in the received ultrasonic transmission signal. These test results are entirely consistent with the theoretical analysis, which confirms the system's high-performance capabilities in detecting internal defects in plywood finger joints.

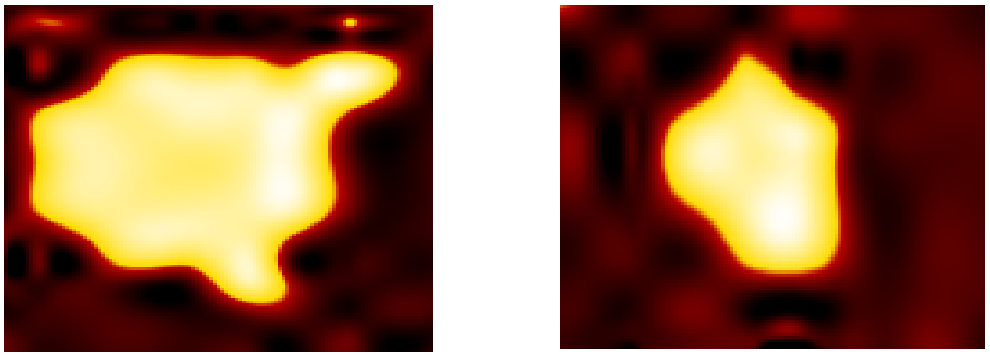

(**a)** Deficiency 1 **(b)** Deficiency 2

Fig. 17. Internal cavity defect detection results of the sample

Modulus of elasticity test results and analyses

For both defect-free and defective specimens, the modulus of elasticity was measured in the direction of the wood grain. The results show that the dynamic modulus of elasticity of all specimens in group W was greater than that of specimens in group Y, with mean values of 8794 MPa and 7349 MPa, respectively. The dynamic modulus of elasticity for the defect-free specimens was 19.6% higher than that for the defective specimens, confirming the accuracy of the system's scanning results.

Additionally, Table 1 indicates that the main factors affecting the difference in elastic modulus between the two groups were the density of the specimens and the first-order bending frequency value. Given nearly identical apparent dimensions, the presence of internal defects, such as voids, knots, and cracks, can reduce the density and first-order bending frequency of the specimen. Obviously, the mechanical results from this study were consistent with the findings from the ultrasonic quality inspection system for glued wood finger-jointed boards using Barker code pulse excitation, thus verifying the accuracy and reliability of the inspection system.

Table 1. Transient Excitation Test Results of Free Plate

Test Item	Length L (mm)	Width (mm)	Tickness h (mm)	Mass m (g)	Density ρ (kg/m^3)	First-order Bend f (Hz)	Modulus of Elasticity E (MPa)
W-1	400	80	8.5	100.4	369	267.5	8855
W-2	400	80	8.68	102.3	368	270.6	8671
W-3	401	80	8.51	104.1	387	262.2	8856
Cov(%)							0.99%
Y-1	400	80	8.47	93	343	250	7241
Y-2	401	80	8.57	98.7	359	250	7474
Y-3	400	80	8.54	95	348	252	7332
Cov(%)							1.3%

CONCLUSIONS

This study was dedicated to the non-destructive testing technology of glued wood finger-joined boards, which has potential to improve the production efficiency and quality inspection level of wooden products and contributes to the saving of wood and promoting

the development of the wood processing industry. The test system used in this study adopts air-coupled ultrasonic technology and incorporates phase coding technology.

1. An ultrasonic inspection system utilizing Barker code pulse excitation was designed specifically for glued wood finger-joined boards. This system integrates both hardware and software components and is equipped with automatic C-scan capabilities for detecting and imaging wood defects. Performance verification tests of the inspection system, alongside mechanical property tests on the inspected plywood finger-joined boards, demonstrated its accuracy and reliability.
2. The dynamic mechanical property tests on the defective plywood finger-joined boards showed results consistent with the expectations of the constructed inspection system, fully verifying the excellent accuracy and high reliability of the system. This dynamic mechanical properties test further establishes the applicability of the testing system for measuring the quality of plywood finger-joined boards, and provides strong empirical support for its effectiveness in practical industrial applications.

Funding

The 2024 Forestry Science and Technology Innovation and Extension Project in Jiangsu Province (LYKJ[2024]05).

REFERENCES CITED

Adegbemileke, S. A., Osuji, S. O., and Ogirigbo, O. R. (2024). "An assessment of the pozzolanic potential and mechanical properties of Nigerian calcined clays for sustainable ternary cement blends," *Sustainable Structures* 4(3), article no. 000057. DOI: 10.54113/j.sust.2024.000057

Ahmad, J., Akula, A., Mulaveesala, R., and Sardana, H. K. (2019). "Barker-coded thermal wave imaging for non-destructive testing and evaluation of steel material," *IEEE Sensors Journal* 19(02), 735-742. DOI: 10.1109/JSEN.2018.2877726

Arkhipov, R., Arkhipov, M., Demircan, A., Morgner, U., Babushkin, I., and Rosanov, N. (2021). "Single-cycle pulse compression in dense resonant media," *Optics Express* 29(7), 10134-10139. DOI: 10.1364/OE.419862

Bruder, L., Wittenbecher, L., Kolesnichenko, P. V., and Zigmantas, D. (2021). "Generation and compression of 10-fs deep ultraviolet pulses at high repetition rate using standard optics," *Optics Express* 29(16), 25593-25604. DOI:10.1364/OE.425053

Cao, M.-T., Xu, F.-Y., Jia, H.-B., Zhou, L., Ji, E.-Y., and Wu, J. (2023). "A multiple interpolation algorithm to improve resampling accuracy in data triggers," *Electronics* 12(06), 12-19. DOI: 10.3390/ELECTRONICS12061291

Corbi, O., Baratta, A., Corbi, I., Tropeano, F., and Liccardo, E. (2021). "Design issues for smart isolation of structures: Past and recent research," *Sustainable Structures* 1(1), article no. 000001. DOI: 10.54113/j.sust.2021.000001

Ghavamirad, R., Sebt, M. A., and Babashah, H. (2018). "Phase improvement algorithm for NLFM waveform design to reduction of sidelobe level in autocorrelation function," *Electronics Letters* 54(18), 1092-1093. DOI: 10.1049/el.2018.5518

Han, G. Y., Li, S. Y., Wang, H. J., Xue, X. X., and Zheng, X. P. (2019). "A microwave photonics equalizer for overcoming dispersion-induced distortions on wideband signals in radio-over- fibre links," *Journal of Lightwave Technology* 37(01), 736-743.

Hu, Q. P., and Guo, X. Y. (2021). "Bending-torsion coupling analysis of thin-walled curved box girders based on spline function," *Journal of Applied Mechanics* 38(03), 1169-1175.

Li, D. Cui, W. C., and Guo, R. M. (2021). "Research on voltage signal acquisition card based on FPGA," *Instrumentation Technology and Sensors* 2021(06), 123-126.

Maldaner, L. F., Molin, J. P., Canata, T. F., and Martello, M. (2021). "A system for plant detection using sensor fusion approach based on machine learning model," *Computers and Electronics in Agriculture* 189, article no. 106382. DOI: 10.1016/j.compag.2021.106382

Murata, Y., and Kaneda, D. (2019). "Study on pulse compression ultrasonic imaging by a stacked m-sequence encoding probe," *Electrical Engineering in Japan* 207(01), 36-42. DOI: 10.1541/ieejeiss.137.1153

Olonisakin, K., He, S., Yang, Y., Wang, H., Li, R., and Yang, W. (2022). "Influence of stacking sequence on mechanical properties and moisture absorption of epoxy-based woven flax and basalt fabric hybrid composites," *Sustainable Structures*, 2022, 2(2), 000016. DOI: 10.54113/j.sust.2022.000016

Parvez, M., Mohammad, A. B., and Ghali V. S. R. (2023). "Deep learning-based sustainable subsurface anomaly detection in Barker-coded thermal wave imaging," *International Journal of Advanced Manufacturing Technology* 127(07-08), 3625-3635. DOI: 10.1007/S00170-023-11753-Y

Sanabria, S. J., Furrer, R., and Neuenschwander, J. (2015). "Analytical modelling, finite-difference simulation and experimental validation of air-coupled ultrasound beam refraction and damping through timber laminates, with application to non-destructive testing," *Ultrasonics* 63, 65-85. DOI: 10.1016/j.ultras.2015.06.013

Shavir, M. N., Biglari, P., Mirzaii, N., Rashmehkarim, R., and Beiranvand, P. (2024). "Investigating crack growth in two-dimensional plates with openings using the peri-dynamic method," *Sustainable Structures* 4(2), article no. 000046. DOI: 10.54113/j.sust.2024.000046

Soner, B., Ulusoy, E., and Tekalp, A. M. (2020). "Realising a low-power head-mounted phase-only holographic display by light-weight compression," *IEEE Transactions on Image Processing* 29, 4505-4515. DOI: 10.1109/TIP.2020.2972112

Wang, Z. H., Wang, Z., Wang, B. J., Wang, Y. L., Rao, X., Liu, B., Wei, P. X., and Yang, Y. (2014). "Dynamic testing and evaluation of modulus of elasticity (MOE) of SPF dimension lumber," *BioResources* 9(3), 3869-3882. DOI: 10.15376/biores.9.3.3869-3882

Wang, Z. H., Gao, Z. Z., Wang, Y. L., Cao, Y., Wang, G. G., Liu, B., and Wang, Z. (2015). "A new dynamic testing method for elastic, shear modulus and Poisson 's ratio of concrete," *Construction and Building Materials* 100, 129-135. DOI: 10.1016/j.conbuildmat.2015.09.060

Wang, Z. H., Wang, Y. L., Cao, Y., and Wang Z. (2016). "Measurement of shear modulus of materials based on the torsional mode of cantilever plate," *Construction and Building Materials* 124, 1059-1071. DOI: 10.1016/j.conbuildmat.2016.08.104

Wang, Z., Xie, W., Wang, Z., and Cao, Y. (2018). "Strain method for synchronous dynamic measurement of elastic, shear modulus and Poisson's ratio of wood and

wood composites," *Construction and Building Materials* 182, 608-619. DOI: 10.1016/j.conbuildmat.2018.06.139

Wang, Z., Xie, W., Lu, Y., Li, H., Wang, Z., and Li, Z. (2019). "Dynamic and static testing methods for shear modulus of oriented strand board," *Construction and Building Materials* 216, 542-551. DOI: 10.1016/j.conbuildmat.2019.05.004

Wang, Y. P., Li, X. Q., and Liu, Y. (2020). "Evaluation and analysis of the effect of different interpolation algorithms on spatial interpolation of air temperature," *Information Technology* 44(06), 31-35. DOI: 10.13274/j.cnki.hdzj.2020.06.008

Wang, Z., and Ghanem, R. (2021). "An extended polynomial chaos expansion for PDF characterization and variation with aleatory and epistemic uncertainties," *Computer Methods in Applied Mechanics and Engineering* 382, article no. 113854. DOI: 10.1016/j.cma.2021.113854

Wang, Z., and Ghanem, R. (2022). "A functional global sensitivity measure and efficient reliability sensitivity analysis with respect to statistical parameters," *Computer Methods in Applied Mechanics and Engineering* 402, article no. 115175. DOI: 10.1016/j.cma.2022.115175

Wang, Z., and Ghanem, R. (2023). "Stochastic framework for optimal control of planetary reentry trajectories under multilevel uncertainties," *AIAA Journal* 61(8), 257-3268. DOI: 10.2514/1.J062515

Wang, Z., Hawi, P., Masri, S., Aitharaju, V., and Ghanem, R. (2023). "Stochastic multiscale modeling for quantifying statistical and model errors with application to composite materials," *Reliability Engineering and System Safety* 235, article no. 109213. DOI: 10.1016/j.ress.2023.109213

Wang, Z. H., and Ghanem, R. (2023). "Stochastic modeling and statistical calibration with model error and scarce data," *Computer Methods in Applied Mechanics and Engineering* 416, article no. 116339. DOI: 10.1016/j.cma.2023.116339

Xu, J. W. (2020). "Analysis and experiment of interpolation method based on python simulation," *Electronic World* 2020(16), 31-32. DOI: 10.19353/j.cnki.dzsj.2020.16.014

Yu, T. H., and Wang, Z. H. (2023). "Model updating of nonproportionally damped structural systems using an adapted complex sum-of-squares optimization algorithm," *Journal of Engineering Mechanics* 149(8), 04023043. DOI: 10.1061/JENMDT.EMENG-6953

Yu, T. H., Wang, Z. H., and Wang, J. F. (2023). "An iterative augmented unscented kalman filter for simultaneous state-parameter-input estimation for systems with/without direct feedthrough," *Mechanical Systems and Signal Processing* 205, 110793. DOI: 10.1016/j.ymssp.2023.110793

Zhang, J. L., Duan, J. P., and Wang, S. Q. (2020). "Design and implementation of measurement and control equivalents based on PCI bus," *Electronic Measurement Technology* 43(16), 114-118. DOI: 10.19651/j.cnki.emt.2004548

Zhou, Y., Huang, Y., Sayed, U., and Wang, Z. (2021). "Research on dynamic characteristics test of wooden floor structure for gymnasium," *Sustainable Structures* 1(1), article no. 000005. DOI:10.19531/j.issn1001-5299.202107003

Article submitted: August 7, 2024; Peer review completed: September 21, 2024; Revised version received: October 20, 2024; Accepted: December 23, 2024; Published: February 25, 2025.
DOI: 10.15376/biores.20.2.2887-2903